Initiation of SCC crack in nickel based weld metals : influence of microstructure features

Elizabeth Chaumun, Jérôme Crépin, Ian de Curières, Cecilie Duhamel, Catherine Guerre, Eva Héripré, Mohamed Sennour

INITIATION OF SCC CRACK IN NICKEL BASED WELD METALS: INFLUENCE OF MICROSTRUCTURAL FEATURES

E. Chaumun[1], J. Crépin[2], I. de Curières[3], C. Duhamel[2], C. Guerre[1], E. Héripré[4], M. Sennour[2]

[1] CEA, DEN, DPC, SCCME, Laboratoire d'Etude de la Corrosion Aqueuse, F-91191 Gif-sur-Yvette, France
[2] MINES Paris Tech, Centre des Matériaux, CNRS UMR 7633, BP 87, F-91003 Evry Cedex, France
[3] IRSN, Institut de Radioprotection et de Sureté Nucléaire, BP 17, 92262 Fontenay-aux-Roses cedex, France
[4] Ecole Polytechnique, Laboratoire de Mécanique des Solides, CNRS UMR 7649, 91128 Palaiseau cedex, France

ABSTRACT

Alloy 82, a nickel based alloy, is used as deposited metal in dissimilar metal welds in Pressurized Water Reactors (PWR). Previous studies dealing with PWSCC (Primary Water Stress Corrosion Cracking) crack growth rate measurement in Alloy 82 highlighted that the crack front consists of isolated intergranular cracks. These uneven crack fronts introduce the question of the effect of the microstructural features on Stress Corrosion Cracking (SCC) behavior. The influence of several parameters, including the chemical composition, metallurgical condition and welding process, on the SCC behavior is studied in order to understand which microstructural parameters are critical for SCC initiation. Microstructural and local mechanical behavior characterization was performed using Electron Back Scattered Diffraction (EBSD) and Digital Imaging Correlation (DIC), and further correlated with SCC initiation sites, showing that SCC cracks are intergranular and propagate perpendicular to the loading direction and that Alloy 82 with lower chromium and carbon contents is more susceptible to SCC. The DIC performed on Alloy 82 welds reveals that the strain field on the surface of U-bend specimens is heterogeneous at several scales (strain field distributions and localization pattern).

Keywords: Stress Corrosion Cracking, Nickel based alloy, Alloy 82 weld metal, Crack initiation, Electron Back-Scattered Diffraction, Digital Image Correlation, Microstructure.

INTRODUCTION

Numerous studies were carried out on nickel based alloys composing some parts of primary loop of Pressurized Water Reactors (PWR). Stress Corrosion Cracking (SCC) is a significant ageing degradation mechanism for major components of PWR. Some nickel based alloys are known to be susceptible to SCC, such as mill-annealed Alloy 600. Many components in PWR are joined by welding using nickel based alloys as deposited metal, such as Alloy 82, Alloy 182, Alloy 52 or Alloy 152.

An international review showed an increase in the cracking cases involving nickel based alloys used in dissimilar metal welds (DMW) since the 90's, after 100.000 hours of reactor operating time [1]. 300 cracking cases in DMW in PWR were listed. More particularly, Alloy 82 used to join low-alloy steel of vessel and stainless steel of piping in primary loop to form a dissimilar metal weld joint, experienced 3 cracking cases, none of which concerned a stress-relieved weld.

Previous laboratory studies on crack growth rate were performed on Alloy 82 in simulated PWR primary water [2], showing that cracking was intergranular and that the crack path was uneven and consisted of isolated cracks along the crack front. Furthermore, crack branching inside and outside the mean crack plane is usually observed. These results lead to the conclusion that crack path depends on

microstructural features.
In this context, this study focuses on the initiation of SCC cracking of Alloy 82 and more particularly on the influence of microstructural parameters on crack initiation. For that purpose, it is necessary to characterize the microstructure of Alloy 82 along with the local strain field in order to correlate them with initiation sites in order to understand which parameters have an influence on the crack initiation.

MATERIAL AND SPECIMEN

Welding Process

To study and simulate welds of PWR, butt welds of Alloy 82 were manufactured by Fouré-Lagadec. The chemical composition of Alloy 82 deposited between two plates of stainless steel (304L) without clamping is given in Table I. Two wires have been used, eleven butt welds were manufactured and two butt welds were used in this study. The butt welds differ by their chemical content: chromium and carbon contents are respectively 19.1% and 0.025% for weld A and 18.1% and 0.014% for the weld B. The difference in chromium content is only of 1%. Nevertheless, Yonezawa et al. showed that a small fluctuation of chromium content has a significant effect on the SCC behavior of nickel based alloys [3].
The welding process used to deposit both alloys was also different. The butt weld A was welded by Gas Tungsten Arc Welding (GTAW) while the butt weld B was welded by Filled Cored Arc Welding (FCAW). The GTAW process parameters were: 180 A/13-14 V for the current, 1 or 1.2 mm for the wire diameter and 10cm/mn of welding speed. The FCAW process parameters were: 200-210A/28-29V for the current, 1.2 mm for the wire diameter and 30 cm/mn for the welding speed. In both cases, the approximate number of beads is 90.

Two out of eleven butt welds have undergone a post-weld heat treatment (PWHT), which aims to reproduce the stress inducing procedure used during the manufacturing of low-alloy steel metal. The conditions of the heat treatment consist of 7h at 600°C with heating and cooling rates of 100°C/hr. The metallurgical condition is then studied to confirm that the heat treatment has both a beneficial effect on the base metal (low-alloy steel) as well as the weld [1]. The effect of the heat-treatment is not presented in this paper.

Both butt welds (A and B) are studied in the as-welded state.

Microstructure and Precipitation

The complex microstructure of Alloy 82 is extremely influenced by the solidification process during the weld. The observed microstructure is anisotropic, composed of millimetric columnar grains containing packs of dendrites slightly misoriented with regard to each other. Figure 1 illustrates the complex microstructure of Alloy 82: it can be seen that each columnar grain cross several beads due to the epitaxial relation.
TEM investigations have been performed to characterize the intragranular and intergranular precipitations. It has been observed that the precipitation is similar for all materials except for the heat treated butt weld A (19.1% Cr) which exhibited nanometric intergranular chromium carbides [4].

Specimens

Parallelepipedic samples of 50x9x1.5 mm^3 were cut from butt welds in order to have the weld in the middle of the sample. All samples were mechanically polished to obtain mirror-polishing with SiC paper up to grade 1200. Then, some were polished with diamond paste up to 1 µm and others up to

colloidal silica suspension (OPS). The samples are machined perpendicular to the dendrite growth direction (TL) (Figure 2). In this case, the surface of the U-bend specimen is perpendicular to the dendrite growth direction. Then the dendrite heads are cut off.

Initiation tests were performed on U-bend specimens. In order to form U-bend specimen, deformed samples were mounted on a threated rod and electrically isolated by oxidized zirconium. A spring was used to maintain the loading during the duration of the test (Figure 3).
Two types of loading history were applied to samples in order to form the U-bend specimens: a direct loading with one step from 0% to +12% of macroscopic deformation and a complex loading with two steps composed of one step from 0% to -2% of macroscopic deformation following by a second step from -2% to +12% of macroscopic deformation. The macroscopic deformation is defined as the change in length divided by the original length and is estimated at the "APEX", which corresponds to the region with maximum deformation for U-bend specimen. The complex loading path is assumed to modify the strain distribution and to enhance localized deformation, therefore possibly increasing the welds susceptibility to SCC.

EXPERIMENTAL PROCEDURES

Microstructure Characterization

The characterization of the microstructure was achieved by Electron Back-Scatter Diffraction (EBSD) analysis allowing for the characterization of the local morphology and grain crystallographic orientation. In order to not disrupt the diffraction of back-scattered electrons in EBSD, the outermost cold worked layer on the surface of the specimen is removed through electro-polishing in an electrolytic solution composed of 20% of orthophosphoric acid and 80% of demineralized water, under a current at 5 V during 15-20 sec at room temperature. Analysis was then performed with an EBSD detector interfaced with a field emission gun FEI QUANTA 600 operating at 20 keV. Observations were made at a magnification of x100 and 20 mm of working distance.
To analyze large surfaces of the welds (from 115 mm² to 180 mm²), crystal orientations were mapped from EBSD experiments performed using 7 µm step size in automatic scanning.
The commercial software connected to the EBSD detector is CHANNEL 5 of HKL, which provides information on both grain orientation and size. Grain boundaries are defined by misorientations greater or equal to 15°.

Local strain field measurements

In order to characterize micromechanical behavior and to measure the local strain field heterogeneities of the material, gold grids of 1.5mm x 1.5mm with a 10µm step size were deposited on the surface and middle of the sample, therefore in the center of the weld by electro-lithography as described by Allais et al [5].
Gold grids were then imaged by SEM before deformation and after each step of the deformation of the U-bend specimen (-2% and +12%).
The same magnification (x77) and working distance (10 mm) were used to acquire the images. Displacement were measured on the images of gold grids before and after deformation and deformation were calculated by Digital Image Correlation (DIC) using the CMV software. The crossing lines of the gold grid were then used as landmark by the DIC [5].

Initiation Tests

SCC initiation tests were performed in a hydrogenated steam environment in a 23 L stainless steel (316L) static autoclaves equipped with a silver-palladium probe to measure the hydrogen pressure. The hydrogenated steam environment is composed of pure demineralized water with a partial pressure of hydrogen (about 800 mbar). The temperature was at 400 °C and the total pressure was 200 bar.
Fifteen U-bend specimens (TL orientation) were mounted on a specimen holder and introduced into the autoclave for exposure times of 1500 hours and 2500 hours.

RESULTS

These results focus on the microstructural characterization of the welds, specifically on the strain maps and on the initiation tests in hydrogenated steam.
The following parameters as chemical content and metallurgical parameters will be compared.
One U-bend specimen for each group of parameters will be described in details. The characteristics of each specimen are listed in Table II.

Microstructures

The analysis of crystal orientation maps performed on each specimen provide information on grain size statistics (area and ratio), crystal orientation, and grain boundary misorientations.
Figure 4 shows the crystal orientation with Inverse Pole Figures coloring following the dendrite axis (S direction).
The crystal orientation map of the U-bend 1 (A82 18%Cr AW) exhibits a crystallographic texture in the major part of the crystal orientation map with the crystal direction [001] parallel to the dendrites growth direction (Figure 4 a.), whereas no crystallographic texture is observed on U-bend 2 (A82 19%Cr AW) (Figure 4 b.).
Figure 5 shows the Pole Figures of each crystal orientation maps with distribution of grain boundaries misorientations and confirms the observations made in Figure 4.
Actually, the Pole Figure of U-bend 1 reveals two superposed textures: a transversal isotropic texture and a cubic texture: both with the [001] direction parallel to dendrite growth direction. Although, there is a tiny texture in Pole Figure {100} for U-bend 2, U-bend 2 does not exhibit clear crystallographic texture.

The distributions of grain boundary misorientations of each crystal orientation map associated with the Pole Figures are presented on the histograms on the right side of the Figure 5. The black curve corresponds to grain boundary misorientations of an isotropic FCC-base crystal, the red distribution corresponds to the misorientation between two arbitrary chosen pixels in the crystal orientation map, whereas the blue distribution corresponds to the misorientation between two pixels side by side. The last distribution of misorientations (blue distribution) corresponding to the U-bend specimen 2 doesn't fit the black curve, which highlights local textures.

Crystal orientations were analyzed by selecting regions of the U-bend sample. Figure 6 presents a region of the crystal orientation map of U-bend 1 with different orientations compared to the center of the map. This region exhibits the same type of texture than the center of the weld but with a deviator angle of roughly 45°.
Figure 7 highlights two regions of U-bend 2; the pole figures show local textures: an isotropic transverse texture type and a cubic texture type for region 1 (the same type of texture as seen in U-bend 1) and the same type of textures with a deviation angle of roughly 45° for region 2.

This deviation, observed in U-bend specimens 1 and 2 at the edge of crystal orientation map, corresponds to the edge of the weld. In this area, the solidification begins on the side of plates manufactured in V shape, which causes a deflected solidification of grains, therefore a deflected crystal orientation.

Grain size statistics were carried out on areas and ratios distribution corresponding to each studied U-bend. The distribution of areas in Figure 8 presents a similar distribution for all the specimens. The distribution shows more small grains between 1 and 5000 μm^2 and a peak of number of grains between 10000 and 50000 μm^2. Only few grains with a size larger than 1 mm^2 are observed.
The ratios distribution shows a difference between U-bend 1 and U-bend 2 around small ratios between 1 and 1.5. Indeed, U-bend 1 (A82 18%Cr AW) exhibits 10% of grains in this last class.
Those observations highlight the fact that the grain population for Alloy 82 with 19% Cr is slightly elongated in comparison to A82 with 18% Cr regarding this orientation.

Strain Fields

Strain fields were measured by Digital Image Correlation (DIC) using deposited gold grids. Eight gold grids have been correlated for each U-bend specimen. These gold grids are located near the APEX of the sample, the zone of maximum of macroscopic deformation (+12%). In this paper, only the strain fields were measured after the final step in the maximum deformation (+12%).
The average deformation of each gold grid correlated for U-bend 1 and 2 is presented in Figure 9. The equivalent strains in the sense of Von Mises are represented in this figure.
All strain fields, except for one, reveal a heterogeneous deformation on the surface of the U-bend specimens, which differs from the assumed average macroscopic deformation at the APEX (12%). This observation shows that the maximum deformation of the APEX could be between the analyzed columns.
The heterogeneity of deformation can be observed at the local scale. Figure 10 shows two strain field maps each corresponding to a U-bend specimen (1 and 2). On these strain field maps, local deformation can be observed with values lower or higher than 12% revealing heterogeneities with local deformation reaching up to 40% and other areas without deformation or a slight deformation.
To summarize, the deformation of the sample leading to the U-bend specimen with 12% of macroscopic deformation at the APEX results in a heterogeneous strain field deformation at the scale of the analyzed columns (1.5 mm) but also at the local scale (20 μm).

Localization of Initiation Sites

The initiation test of U-bend specimen with TL orientation was interrupted at 1500 hours and 2500 hours of exposure to a hydrogenated steam environment, with the first sign of cracks, appearing after 1500 hours. These observed cracks are intergranular and perpendicular to the loading direction.
Table III shows all TL U-bend specimens tested with parameters of each specimen and the number of intrinsic cracks.

We can see that all U-bend specimens (without heat treatment) with 18%Cr content presented cracking in comparison to U-bend specimens with 19% Cr content, whereas none of the heat treated U-bend specimens presented cracking after 2500 hours.

DISCUSSION

The correlation between the microstructure, the strain field at the U-bend specimen surface and the localization of SCC cracks initiation was used to determine the microstructural parameters affecting the initiation of SCC cracks in Alloy 82. In this paper, correlations have been performed on two types of Alloy 82 with different chromium contents and welding processes: one which contains 18% Cr welded using the FCAW technique and the second containing 19% Cr welded using the GTAW technique.

The microstructure characterization with EBSD showed a difference between both alloys in terms of morphology and crystallographic orientation. Alloy 82 with 18% Cr exhibited a crystallographic texture: cubic and transversal isotropic, with the [001] direction of the crystal being parallel to the dendrites growth direction. This observation is consistent with the conclusion given by David et al [6]. Compared to Alloy 82 with 18% Cr, Alloy 82 with 19% Cr does not exhibit a crystallographic texture. The morphology of both welds is textured in the dendrites growth direction with a heterogeneous grain size. Regarding the morphological ratio, there is a slight difference between both alloys: the Alloy 82 with 18% Cr presents more grains with a tiny ratio (1 to 1.5) compared to the Alloy 82 with 19% Cr.
For the alloy with 19% Cr, the grains are more elongated along the welding direction (S). This could be explained by the welding speed which is three times faster than that used for the alloy contain 18% Cr. According to [6,7], the cooling speed of the weld pool in the fusion zone could modify significantly the microstructure and the morphology of grains.
Moreover, the chemical composition, regarding the chromium and carbon content, could modify the precipitation of chromium carbides [4].
To confirm that the chemical composition is not involved in the morphology and the crystallographic orientation of the microstructure during the solidification, a new butt weld could be manufactured from a 19% Cr Alloy 82 wire with the FCAW process.

The characterization of local strain field of the specimen revealed heterogeneous deformation distributions on surfaces. These heterogeneous deformation distributions were measured at two scales: 1.5 mm (between two gold grids) and at a local scale (20 μm). To better understand the reasons of this heterogeneous strain field on the surface, correlations between strain fields and the microstructure have been performed.

The correlations of strain fields with the EBSD analyses of U-bend 1 (Alloy 82 with 18% Cr) and U-bend 2 (Alloy 82 with 19% Cr) are respectively shown in Figure 11 and 12. In these figures, we can see the strain fields next to the corresponding areas of EBSD analyses with the legend of Inverse Pole Figures following the S axis (dendrites growth direction).
On U-bend 1, the first column of the strain field is localized in an area composed of small grains and the second column in an area composed of large grains. In comparison, U-bend 2, Figure 12, does not show small grains region localized on only one side of the analyzed area. The distribution of the deformation in strain fields with larger grains is more homogeneous in U-bend 1 than U-bend 2. In some cases, we can see that the maximum deformation is localized between small grains or between two grains with different crystallographic orientations considering the crystallographic orientation maps following the S axis, whereas in other cases, the maximum of deformation could be observed in both alloys between two grains with close crystallographic orientations.

EBSD maps with Schmid factor for {111} <110> slip system have been performed on U-bend 1

(Figure 13) and on U-bend 2 (Figure 14). Schmid factor calculation reveals that in both cases grains are favorable to dislocation slip. The correlations with strain field maps showed that the maximum of deformation is not only localized between two grains with a high difference of Schmid factor.

The third axis of the study concerns the correlation between the initiation of SCC cracks with the microstructure and strain fields. Cracks obtained after 2500 hours of testing are highlighted using white in Figures 11 and 12, and using red in Figures 13 and 14. SCC cracks are perpendicular to the loading direction. They are localized in U-bend 1 in areas composed of small grains and in most cases between two grains with different crystallographic orientations. For U-bend 2, the SCC cracks are also perpendicular to the loading direction except for two cracks. Contrary to U-bend 1, cracks are also present between two large grains and between grains with similar crystallographic orientations. Considering the Schmid factor for both alloys, SCC cracks do not seem to be localized between grains with a high discrepancy of Schmid factor. When correlated with the strain fields, it is shown that deformation maximum does not always result in SCC cracks and that areas with a lower localized deformation can result in SCC cracks. From these observations, it is demonstrated that the localization of deformation is not a necessary condition for the initiation of SCC cracks and other mechanical parameters need to be considered, for example the localization of stress. In order to better understand the stress fields, numerical simulations must be performed as stress cannot be measured directly in-situ on SCC specimen.

As for the strain fields, the microstructure characterization does not lead to the conclusion that only one systematic parameter results to the initiation of SCC cracks. For example, for U-bend 1 (A82 with 18% of chromium), the fact that cracks appear between two grains with different crystallographic orientation seems to be a needed condition but it is not the case for U-bend 2 (A82 with 19% of chromium).
In order to explore more parameters and to select those most important SCC initiation, a systematic analyze of more parameters (grain boundary misorientation, etc…) will be performed on several specimens, and related to EBSD analyses.

CONCLUSION

The characterization of the microstructures and the local mechanical behavior of Alloy 82 with 18% Cr content, welded by FCAW, and with 19% Cr content, welded by Gas GTAW, were correlated to the localization of SCC crack initiation. Initiation tests were performed in hydrogenated steam at 400°C, 200 bar, and with 0.7 bar of hydrogen partial pressure. SCC cracks have been observed after 1500 hours of initiation test and intergranular cracks were perpendicular to the loading direction for both alloys.
The correlation of the microstructure, the local mechanical behavior and the localization of initiation highlighted:

- A difference between both alloys in terms of grains morphology and crystallographic orientation. However, SCC cracks have been observed preferentially in small grains areas in the case of Alloy 82 with 18% Cr. In Alloy 82 with 19% Cr, it seems that SCC cracks initiation is not related to a particular population of grains. Misorientation between grains around the SCC cracks seems to be significant in the case of the U-bend 1 unlike the U-bend 2.
- A heterogeneous deformation on the surface of U-bend specimens. The average deformation between strain field maps is different, and a heterogeneous deformation can be observed inside each strain field maps. The localization of SCC cracks correlated to the

strain fields seems to show that the localization of the deformation is not sufficient to anticipate the initiation of cracks.

Other microstructural parameters will be investigated in order to determine the combination of microstructural parameters which are involved in the initiation of SCC cracks and to model the SCC phenomenon.

This process of characterizations of the material will be performed on other U-bend specimens in TL and TS orientation, but also on other alloys such as Alloy 182 and Alloy 52.

REFERENCES

[1] Materials Reliability Program: Review of Stress Corrosion Cracking of Alloys 182 and 82 in PWR Primary Water Service (MRP-220). EPRI, Palo Alto, CA : 2007. 1015427

[2] C. Guerre, C. Duhamel, M. Sennour, J. Crépin, M. Le Calvar, SCC crack growth rate of Alloy 82 in PWR primary water conditions-effect of a thermal treatment, presented at the 15th international conference on environmental Degradation of Materials in Nuclear Power Systems-Water Reactors, Colorado Springs, Colorado, August 7 – 11, 2011

[3] T. Yonezawa, K. Onimura, Effect of chemical composition and microstructure on the stress corrosion cracking resistance of nickel based alloys, presented at EPRI meeting on Intergranular Stress Corrosion Cracking Mechanisms (Washington DC), April 27 – May1, 1987, Electric Power Research Institute

[4] M. Sennour, E. Chaumun, J. Crépin, C. Duhamel, F. Gaslain, C. Guerre, I. de Curières, TEM investigation on the effect of chromium content and of stress relief treatment on precipitation in Alloy 82, submitted on March 2013 at the Journal of Nuclear Material

[5] L. Allais, M. Bornert, T. Bretheau and D. Caldemaison. Experimental characterization of the local strain field in a heterogeneous elastoplastic material. Acta Metall. Mater. 42, 11, 1994, p. 3865–3880.

[6] S.A. David, S.S. Babu, and J.M. Vitek, Welding: Solidification and microstructure, Journal of minerals, volume 55, Issue 6, June 2003

[7] V. Robin, De la modélisation numérique des procédés et du soudage en particulier au comportement mécanique des assemblages, PhD Thesis, Ecole Nationale Supérieur des Mines de Saint-Etienne : 2009

TABLES

Table I: Chemical compositions of A82 welds with the RCC-M code

	C	S	Si	Mn	Ni	Fe	Cu	Cr	Nb	Ti	P	Co	Mo	O
butt weld A	0.025	<0.001	0.07	2.57	71.7	3.07	<0.01	19.12	2.41	0.1	0.004	0.04	0.02	0.0016
butt weld B	0.014	0.017	0.17	2.88	72.9	2.3	<0.01	18.15	2.83	<0.01	0.002	0.01	0.05	0.067

Table II: Characteristics of U-bend specimens 1, 2 and 3

	Metallurgical state	Chromium content
U-bend 1	As-welded	≈ 18%
U-bend 2	As-welded	≈ 19%

Table III: Number of intrinsic cracks of U-bend specimen after 2500 hours of initiation test with parameters

	U-bend specimen	% of chromium	metallurgical condition	loading	surface condition	number of intrinsic cracks
With gold grids	**EP921 (U-bend 2)**	**19%**	**As-welded**	**complex**	**OPS**	**35**
	EP922	19%	As-welded	complex	1µm	7
	EP899	19%	Heat treated	complex	OPS	-
	EP900	19%	Heat treated	complex	1µm	-
	EP990	18%	As-welded	complex	OPS	19
	EP991 (U-bend 1)	**18%**	**As-welded**	**complex**	**1µm**	**32**
	EP992	18%	As-welded	direct	1µm	28
	EP993	18%	As-welded	direct	OPS	6
Without gold grids	EP918	19%	As-welded	complex	1µm	-
	EP906	19%	Heat treated	complex	1µm	-
	EP919	19%	As-welded	direct	OPS	-
	EP920	19%	As-welded	direct	1µm	-
	EP925	19%	As-welded	direct	1µm	1
	EP908	19%	Heat treated	direct	1µm	-
	EP913	19%	Heat treated	complex	OPS	-

FIGURES

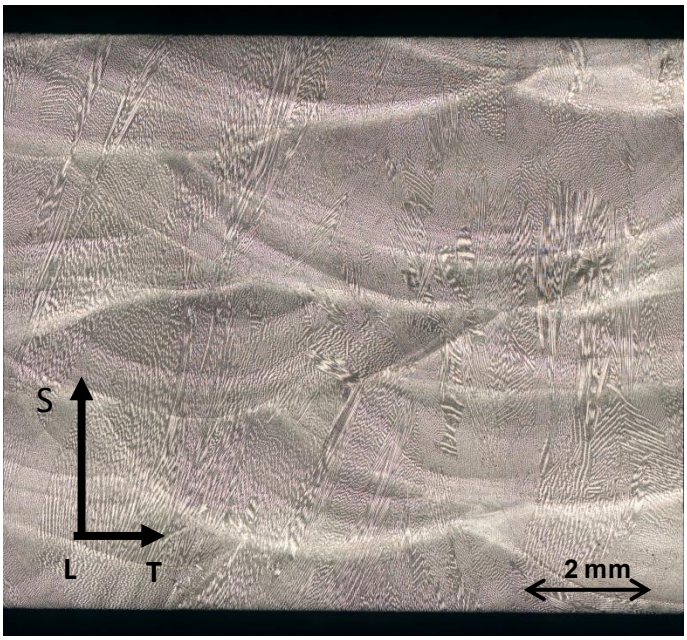

Figure 1: Microstructure of A82 by optical microscopy

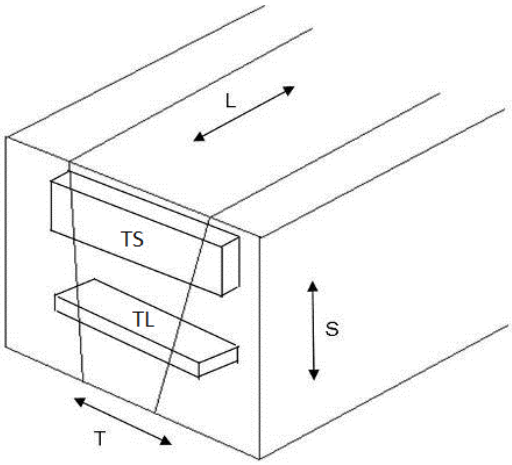

Figure 2: Scheme of taking orientation in welds of samples

Figure 3: Photography of a U-bend specimen

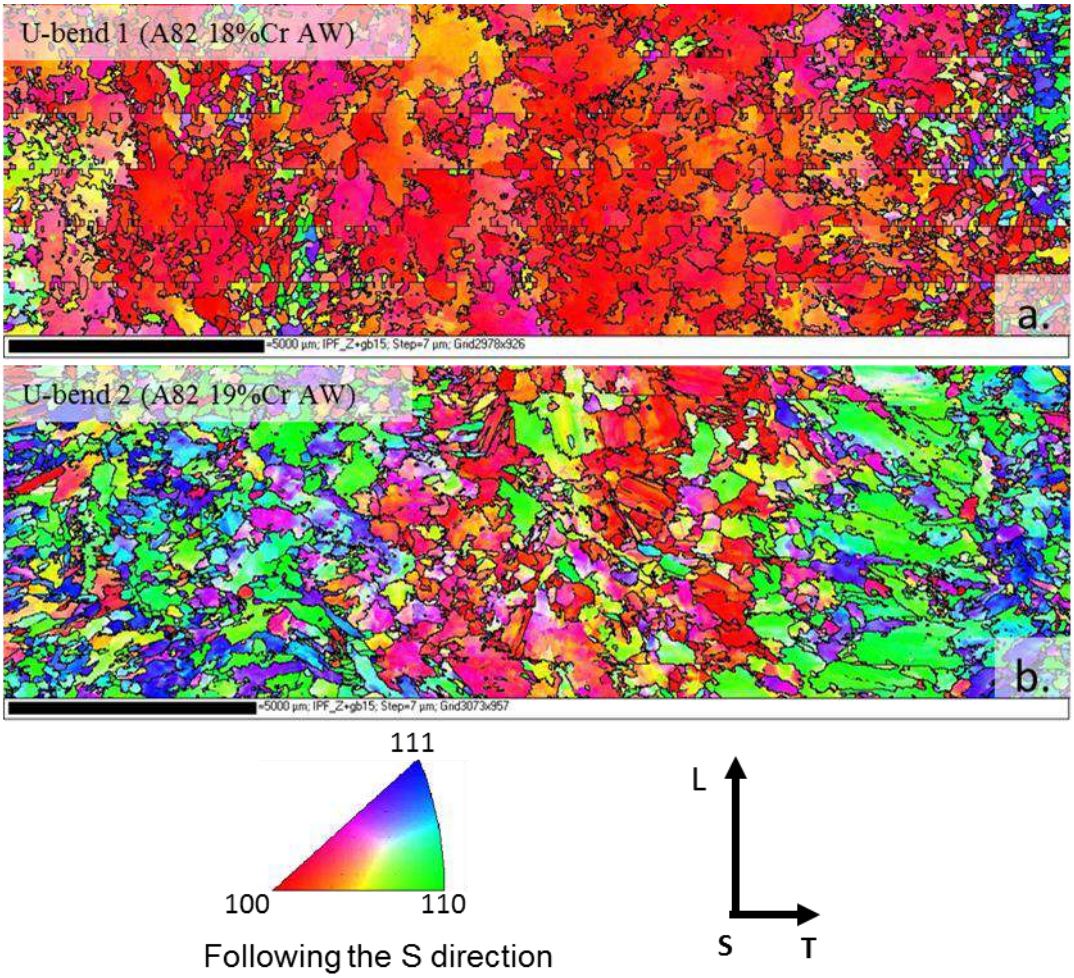

Figure 4: Crystal orientation maps of U-bend 1 (a.) and U-bend 2 (b.)

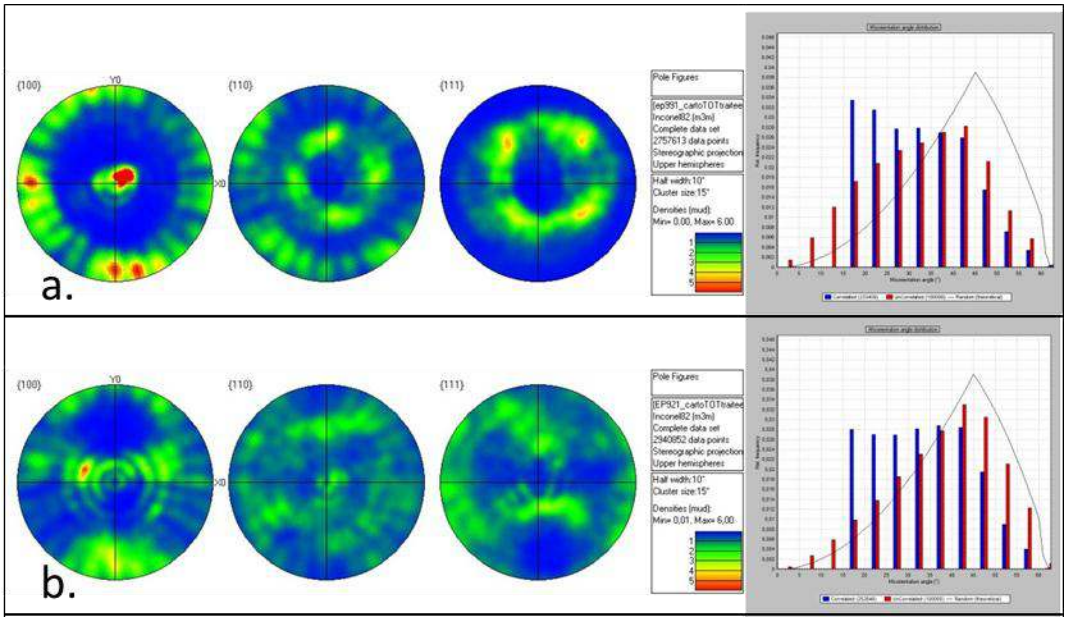

Figure 5: Pole Figures associated with distribution of misorientation angle of grain boundaries of U-bend 1 (a.) and U-bend 2 (b.)

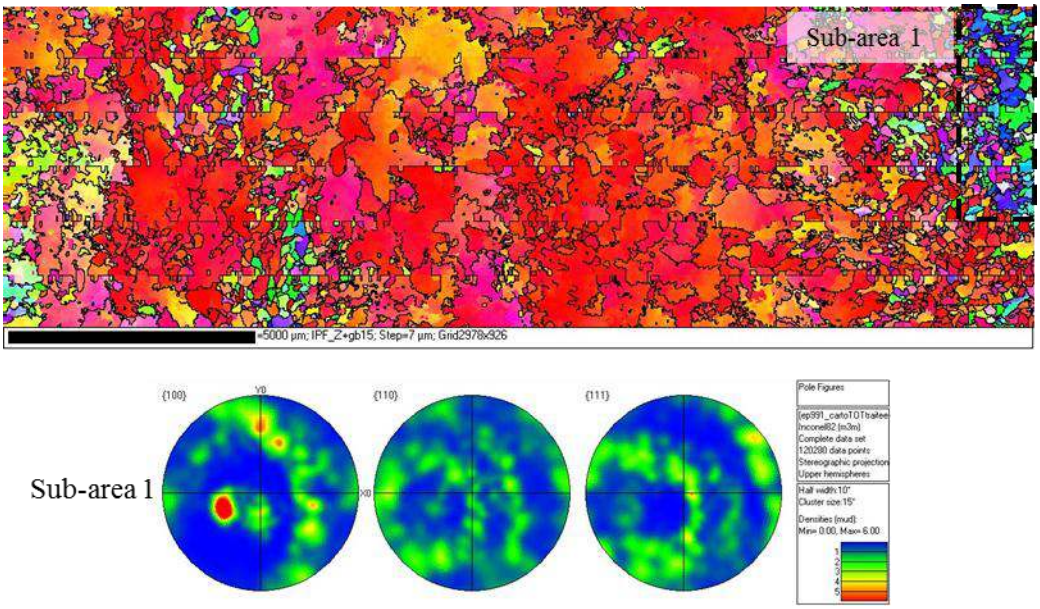

Figure 6: Crystal orientation map of A82, U-bend 1, with Pole Figure of sub-areas

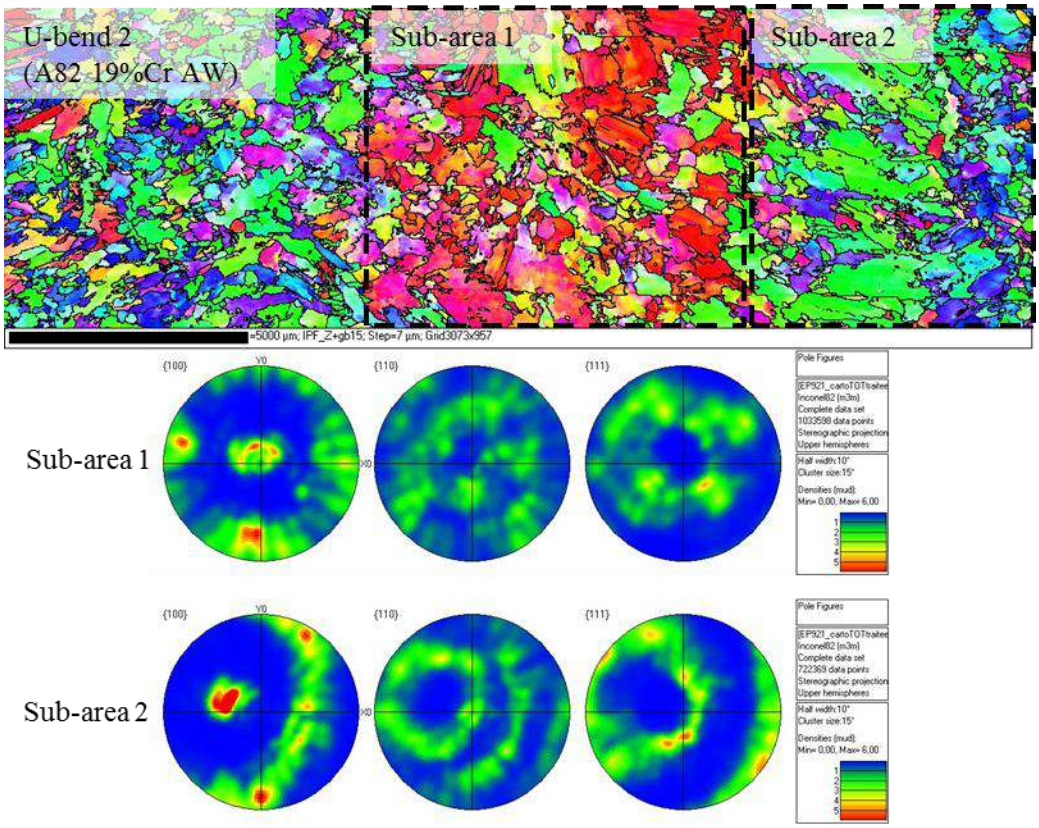

Figure 7: Crystal orientation map of A82, U-bend 2, with Pole Figure of sub-areas

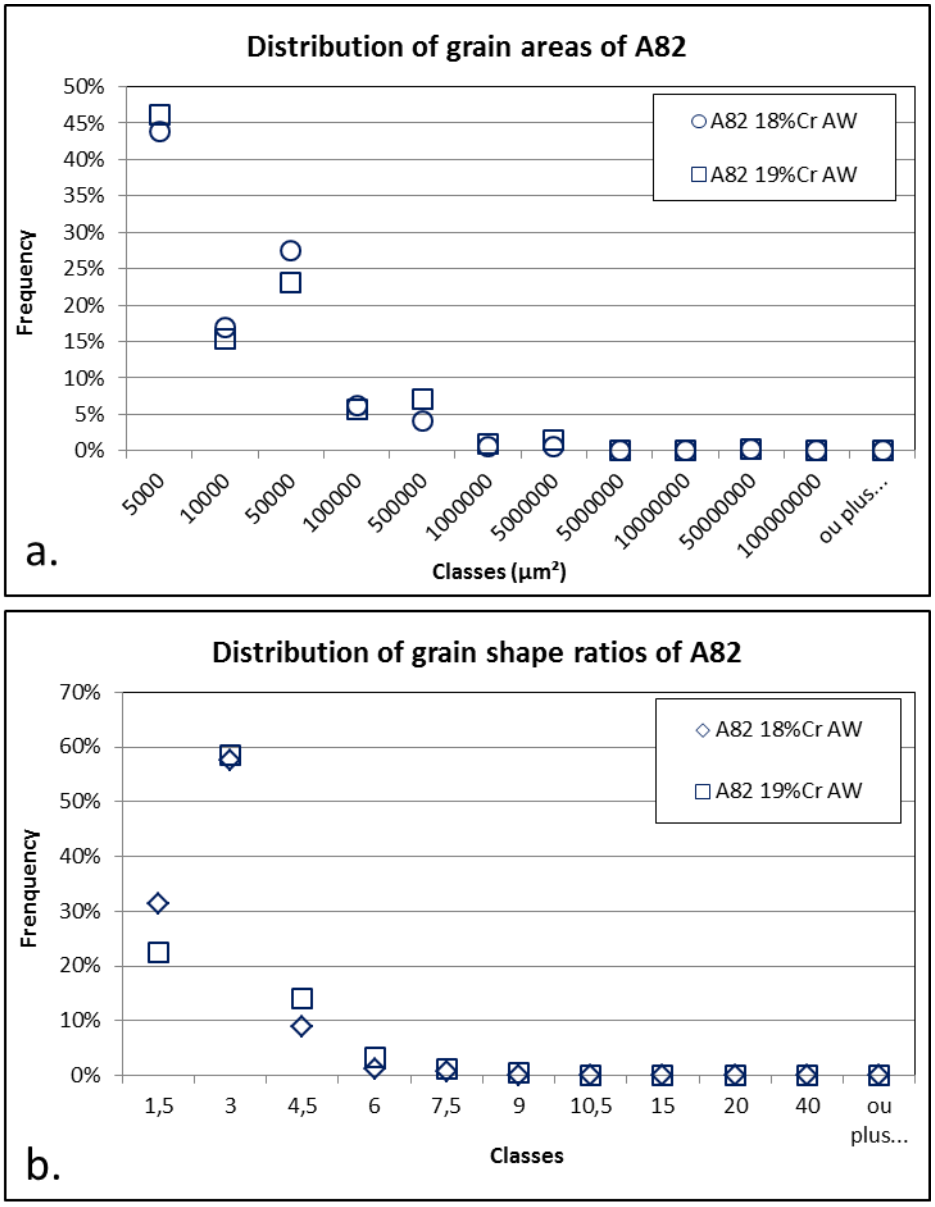

Figure 8: Distribution of (a) grain areas and (b) shape ratios of A82 18%Cr and A82 19%Cr

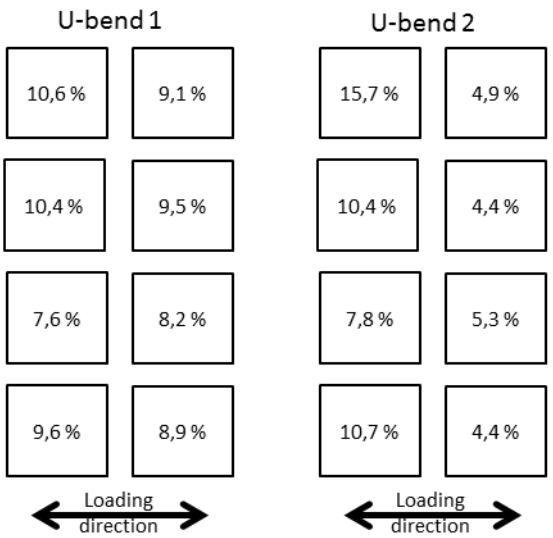

Figure 9: Average deformations of each strain fields of U-bend 1 and U-bend 2 (gold grid size: 1.5x1.5 mm²)

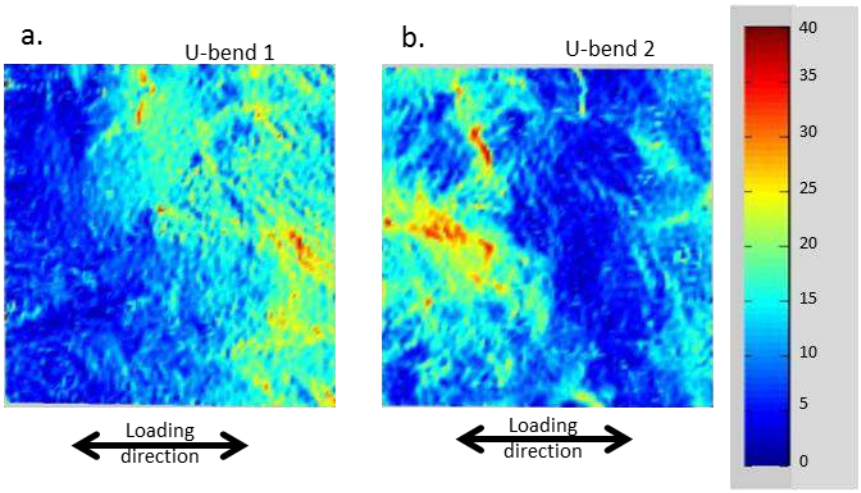

Figure 10: Examples of equivalent strain of the U-bend specimen 1 (a.) and U-bend specimen 2 (b.), strains in % and gold grid size 1.5x1.5 mm²

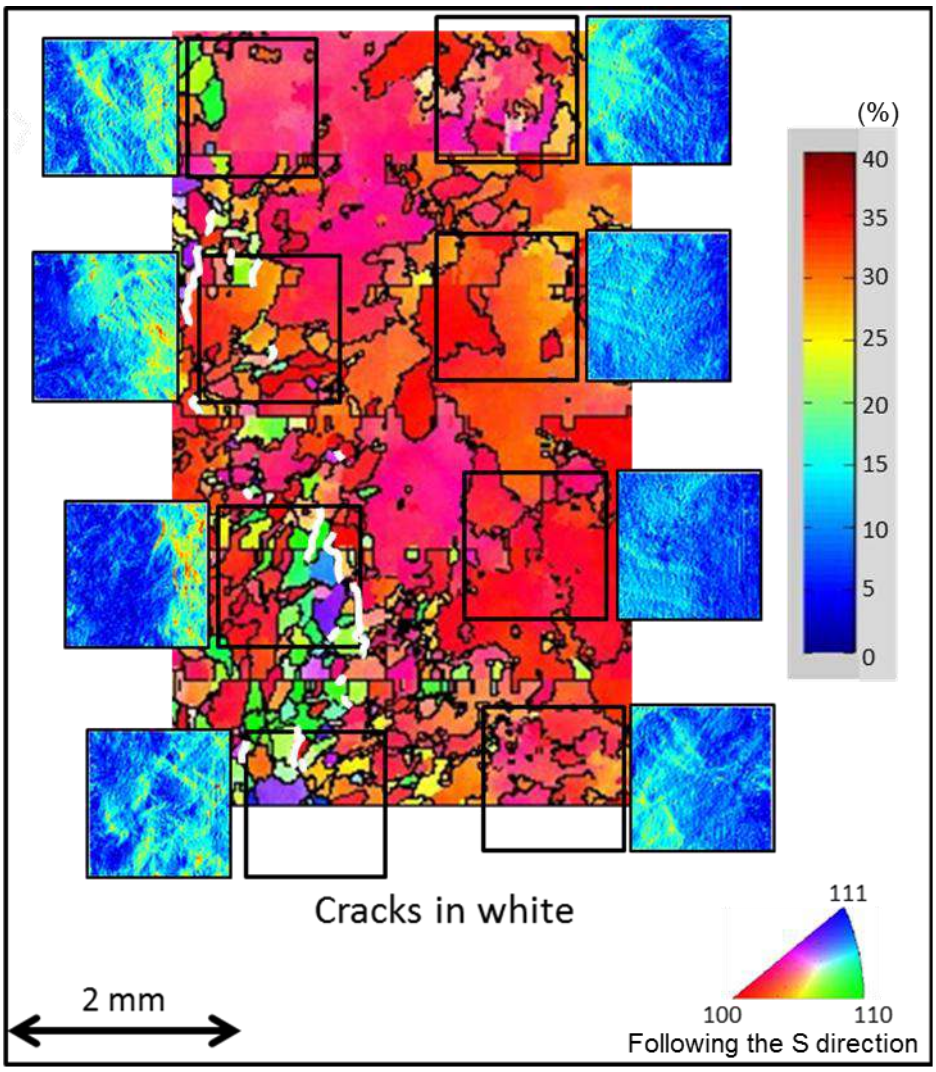

Figure 11: Correlation of the microstructure with EBSD analyses indexed with the IPF colouring, the strain fields (equivalent strains) and the SCC cracks obtained after 2500 hours of initiation test (in white) on U-bend 1 (A82 with 18% of chromium)

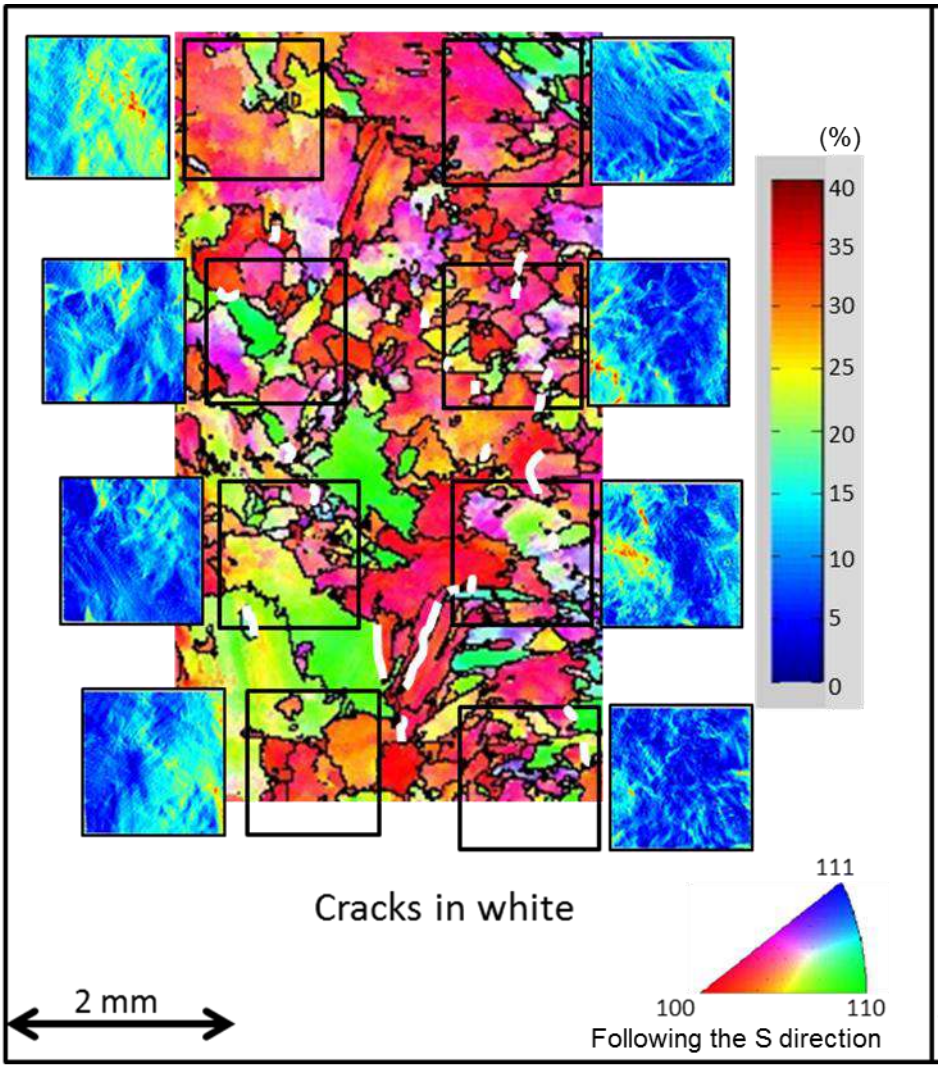

Figure 12: Correlation of the microstructure with EBSD analyses indexed with the IPF colouring, the strain fields (equivalent strains) and the SCC cracks obtained after 2500 hours of initiation test (in white) on U-bend 2 (A82 with 19% of chromium)

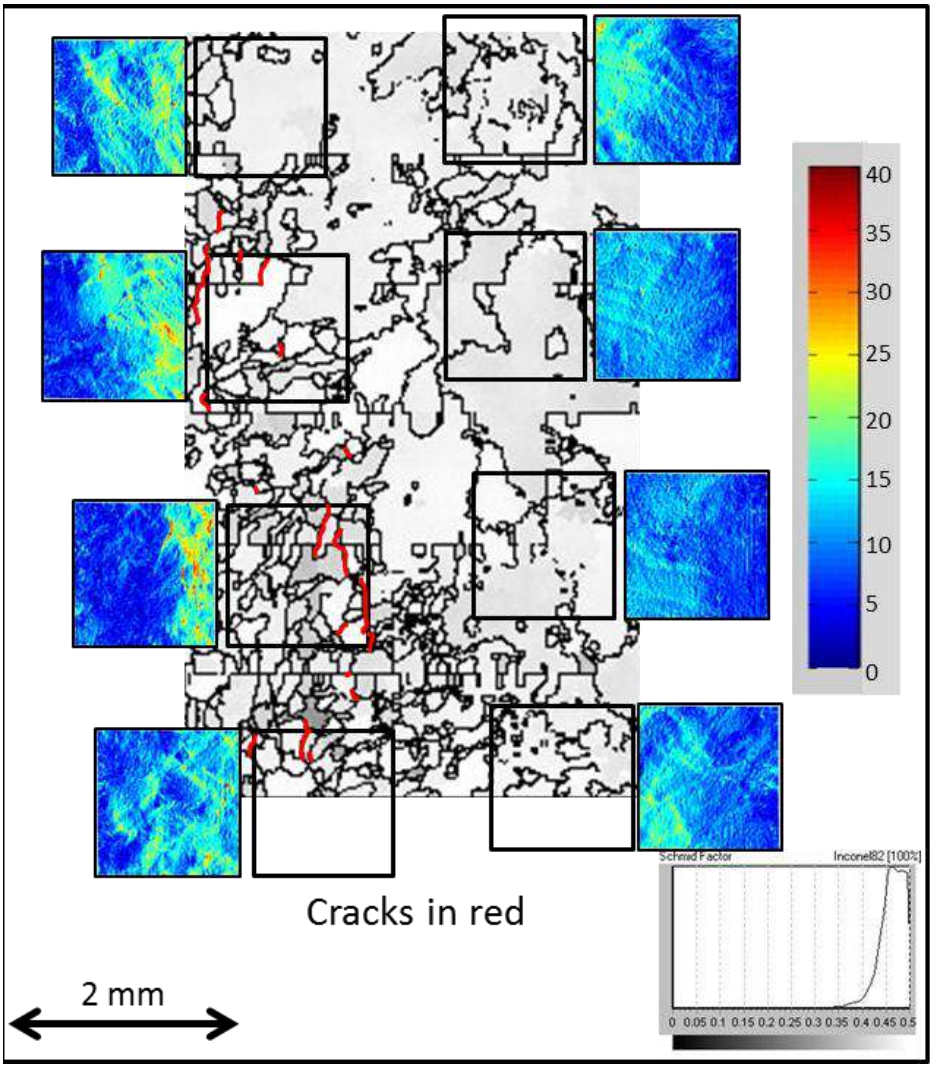

Figure 13: Correlation of the microstructure with EBSD analyses indexed with grey scale of Schmid factor (octahedral) for {111} <110> slip system, the strain fields (equivalent strains) and the SCC cracks obtained after 2500 hours of initiation test (in white) on U-bend 1 (A82 with 18% of chromium)

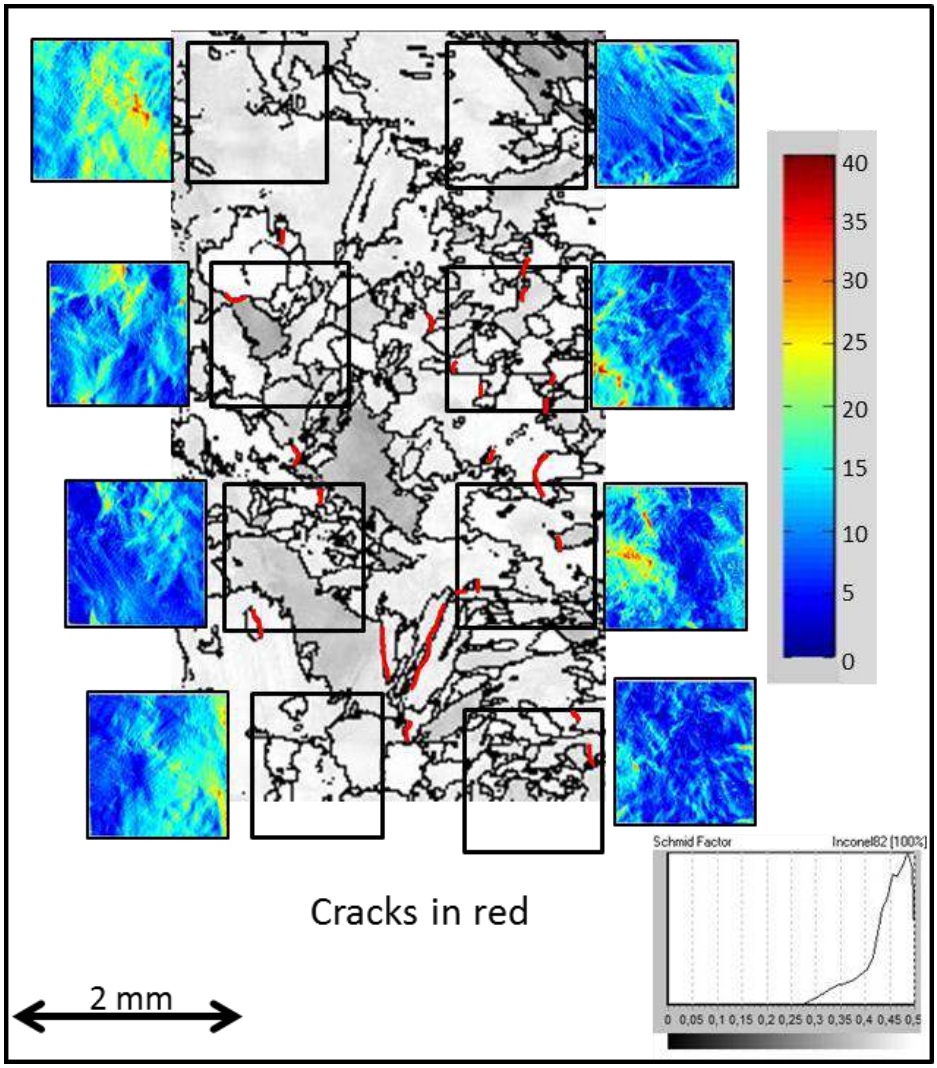

Figure 14: Correlation of the microstructure with EBSD analyses indexed with grey scale of Schmid factor (octahedral) for {111} <110> slip system, the strain fields (equivalent strains) and the SCC cracks obtained after 2500 hours of initiation test (in white) on U-bend 2 (A82 with 19% of chromium)